Simple Quantification of Benzodiazepine Receptor Binding and Ligand Transport Using Iodine-123-Iomazenil and Two SPECT Scans

Yoshihiro Onishi, Yoshiharu Yonekura, Takao Mukai, Sadahiko Nishizawa, Fumiko Tanaka, Hidehiko Okazawa, Koichi Ishizu, Toru Fujita, Hiroshi Shibasaki and Junji Konishi

Nihon Medi-Physics Co., Ltd., Hyogo, Japan; Kyoto University School of Medicine, Kyoto, Japan; and Kyoto College of Medical Technology, Kyoto, Japan

The feasibility of simplified procedures for the quantification of benzodiazepine receptor binding using [^{123}I]iomazenil and SPECT was assessed. **Methods:** Six normal male volunteers were studied. Following intravenous injection of 111 MBq [^{123}I]iomazenil, serial dynamic SPECT scanning was performed for 120 min and the concentration of lipophilic compounds in the arterial plasma was determined by chloroform extraction. Kinetic parameters were estimated by a curve-fitting procedure using the following four models: three-compartment, four-parameter (K1-k4) (3C4P), three-compartment, three-parameter (fixed K1/k2) (3C3P), three-compartment, two-parameter (fixed K1/k2 and k4) (3C2P) and two-compartment, two-parameter (K1 and k2) (2C2P). Kinetic parameters were also calculated by a table look-up procedure with 3C2P using only two SPECT data acquisitions. Parametric images were generated based on the same procedure. **Results:** In all models, the curve-fitting procedure gave similar outcomes for ligand transport (K_1) and receptor density parameters (i.e., binding potential or distribution volume). The 3C4P parameters showed significant correlation between k_2 and k_3, while 3C3P did not show such a correlation, suggesting the stability of 3C3P. The 3C2P provided parameters essentially identical to those with the 3C3P, indicating the suitability of this model, while 2C2P gave similar distribution volume but obviously low K_1. **Conclusion:** Table look-up procedures based on the 3C2P model permit quantification of benzodiazepine receptor binding using [^{123}I]iomazenil with two SPECT scans. This method may be of clinical value in the diagnosis of various diseases.

Key Words: iodine-123-iomazenil; compartmental model analysis, benzodiazepine receptor, single-photon emission computed tomography; ligand transport

J Nucl Med 1995; 36:1201–1210

Iomazenil, an iodinated ligand for central-type benzodiazepine receptors, is an analog of flumazenil, which has been used for PET studies to investigate benzodiazepine receptors (*1,2*). Iomazenil has favorable characteristics for in vivo assessment of benzodiazepine receptors with SPECT such as: high brain uptake, little nonspecific binding, high affinity for benzodiazepine receptors and no intrinsic pharmacological effects at tracer doses (*3–6*).

Various SPECT studies have demonstrated the clinical feasibility of [^{123}I]iomazenil for the assessment of benzodiazepine receptors in the living human brain (*7–12*). Evaluation of the SPECT images, however, has been performed mainly by visual inspection of the differences from blood flow images or by semiquantitative approaches such as the ratio of activities in regions of interest (ROIs). The tissue activity of iomazenil is determined on the basis of at least two independent factors, i.e., ligand transport and receptor density/affinity, and as such, it is desirable to assess these factors separately.

Quantitative assessment of benzodiazepine receptors has been carried out using [^{11}C]flumazenil and PET, as well as [^{123}I]iomazenil and SPECT, with multiple injections of the ligand and the equilibrium method (*13–20*) or with a single injection and compartmental model analysis (*21–26*). The former provides receptor density (B_{max}) and affinity (K_D), while the latter gives ligand transport (K_1) and the binding potential which is derived as B_{max}/K_D (*27*). The latter approach appears to be more applicable in clinical studies using iomazenil since its affinity is 10-fold higher than that of flumazenil (*3*) and only a single injection is required. Standard compartmental analysis, however, generally requires rapid serial data acquisition for a long period and its application to routine clinical studies is limited. Since imaging with [^{123}I]iomazenil itself can be performed with conventional SPECT devices, simplified techniques for quantitative assessment which do not require rapid serial SPECT acquisition would be particularly useful.

In this study, we assessed the feasibility of such a simplified technique using a two-parameter compartment model that can determine receptor density and ligand transport with only two SPECT scans.

Received Jul. 1, 1994; revision accepted Nov. 10, 1994.

For correspondence or reprints contact: Yoshihiro Onishi, Nihon Medi-Physics Co., Ltd., Hyogo, Japan, 9-8 Rokutanji-cho, Nishinomiya City, Hyogo Pref., 662 Japan.

METHODS

Subjects

Six normal healthy male volunteers (aged 24–61 yr; weight, 53–79 kg) were studied. No subject had a history of brain disease, psychiatric illness or abnormal findings in physical examinations, routine laboratory tests, EEG or x-ray CT. All subjects gave written informed consent before the study and received potassium iodide to minimize thyroid uptake of free radioactive iodine.

Data Acquisition

Radiopharmaceuticals. Iodine-123-iomazenil was supplied by Nihon Medi-Physics Co., Ltd. (Hyogo, Japan). Each vial contained 111 MBq ^{123}I and 0.5 μg (1.2 nmole) iomazenil. The specific activity was 2500 Ci/mmole, and the radiochemical purity was greater than 95%.

Study Protocol. The study was approved by the Institutional Review Board of Kyoto University Hospital. Each subject received 111 MBq [^{123}I]iomazenil intravenously as a bolus within a few seconds. Arterial blood samples were drawn manually at 5-sec intervals for the first 40 sec and subsequently at 50 sec and 1, 1.5, 2, 3, 5, 10, 20, 30, 60 and 120 min. The SPECT data were acquired every minute for 120 min using a triple-head rotating gamma camera with high-resolution, fanbeam collimators and 159 keV ± 10% of the photo window in a continuous rotating mode (40 steps/120°/60 sec).

Arterial Plasma Analysis. After separation of the plasma by centrifugation, the lipophilic activity in the plasma was estimated by chloroform extraction. The chloroform extraction procedure was conducted as follows:

1. Chloroform (1 ml) and saline (2 ml) were put into a glass tube to which 0.5 ml of radioactive plasma was added.
2. After stirring, the aqueous fraction was removed and an additional 2.0 ml of saline were added.
3. The mixture was stirred, and the aqueous fraction was again removed.

Preliminary experiments confirmed that this procedure yielded extraction rates of 97.3% and 0% for iomazenil and the de-esterified compound, respectively. The results of chloroform extraction are listed in Table 1.

Free fraction of iomazenil (f_1) was determined in vitro in a similar manner to Zoghbi et al. (*28*). After aliquots of [^{125}I]iomazenil were added to the plasma sample from each subject, the protein-bound fraction was determined by ultrafiltration with Ultrafree-C3 (Nihon Millipore Ltd., Tokyo, Japan) at 37° centigrade. The f_1 value for the six subjects was estimated to be 0.24 ± 0.02 (mean ± 1 s.d.), which is compatible with the previously reported value of 0.23 (*25*). The fixed value of 0.24 for f_1 was used throughout this study.

Image Reconstruction and ROIs. The raw projection data were added to make a total of 27 images (ten 2-min, nine 4-min and eight 8-min images). SPECT images were reconstructed by a filtered backprojection algorithm with a Butterworth filter (cutoff frequency: 0.25; power factor: 4) and displayed on a 64 × 64 matrix. The pixel size was 4.5 × 4.5 mm, and the slice thickness was 7.1 mm. Attenuation correction was performed by assuming elliptical outline of the head in each slice and uniform attenuation in the head (μ = 0.06).

Camera sensitivity was measured using a cylindrical phantom (16 cm diameter and 12 kBq/ml of ^{123}I) and the same acquisition and reconstruction mentioned above. A calibration coefficient of 29.16 cpm/kBq was derived and the value was confirmed to be stable during these studies by separate phantom studies. The attenuation coefficient μ was empirically derived as the profile curves of reconstructed images of the cylindrical phantom were flat.

ROIs were outlined in three representative SPECT images corresponding to the level of the centrum semiovale (slice 1), basal ganglia (slice 2) and cerebellum (slice 3). Irregular shaped ROIs were placed on the frontal cortex (frontal 1), parietal cortex and white matter/ventricle (WMV) in slice 1; frontal cortex (frontal 2), temporal cortex, occipital cortex, thalamus and striatum in slice 2 and the cerebellum and pons in slice 3. The average radioactivities of the left and right hemispheres in each region were used for calculation (except for the pons).

TABLE 1
Chloroform Extraction Ratio from Arterial Plasma

Time after injection	Chloroform extraction ratio* (%)
30 sec	92.5 (4.1)
40 sec	92.9 (1.8)
50 sec	90.1 (5.4)
1 min	91.2 (1.8)
1.5 min	88.2 (2.6)
2 min	82.4 (6.5)
3 min	57.2 (6.6)
5 min	30.6 (5.2)
10 min	16.4 (2.3)
20 min	12.3 (1.2)
30 min	11.2 (1.0)
60 min	10.2 (1.4)
120 min	9.0 (1.7)

*n = 6, mean (s.d.).

Data Analysis

Compartmental Model Analysis. Quantitative analyses were performed using the three- and two-compartment models as described for [^{11}C]flumazenil (*21*) and [^{123}I]iomazenil (Fig. 1) (*25*).

The three-compartment model consists of the plasma compartment (C_a), the nondisplaceable tissue compartment (C_2) in which the ligand can be free or nonspecifically bound and the specifically bound compartment (C_3). Two major assumptions were made to derive the equations below: (a) the equilibration of nonspecific binding with the free ligand in compartment 2 is rapid compared to the other processes and (b) ligand transport across the blood-brain barrier (BBB) is based on passive diffusion.

The concentration of the lipophilic fraction in the plasma is equal to that in the nondisplaceable compartment at equilibrium:

$$f_1 C_a = f_2 C_2, \qquad \text{Eq. 1}$$

where f_1 is the free fraction of the parent compound in the plasma and f_2 is the ratio of the free fraction to the total ligand concentration in compartment 2. The equilibrium distribution volume of the nondisplaceable compartment is:

$$V_2 = \frac{C_2}{f_1 C_a}, \qquad \text{Eq. 2}$$

resulting in an inverse relationship between f_2 and V_2:

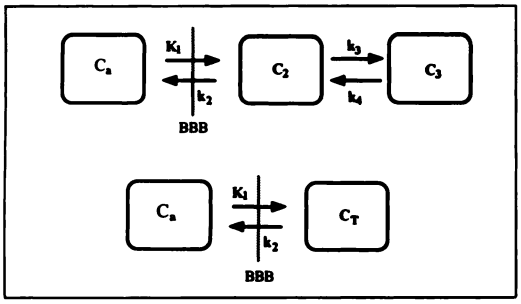

FIGURE 1. Top: The three-compartment model where C_a is the arterial plasma compartment, C_2 is the free and nonspecific binding compartment and C_3 is the specific binding compartment. Bottom: The two-compartment model where C_T is the tissue compartment, including free, nonspecific and specific binding. K_1-k_4 represent the rate constants describing ligand exchange.

$$f_2 = \frac{1}{V_2}. \qquad \text{Eq. 3}$$

The ligand concentration in each compartment is given by:

$$\frac{dC_2(t)}{dt} = K_1C_a(t) - (k_2 + k_3)C_2(t) + k_4C_3(t), \qquad \text{Eq. 4}$$

$$\frac{dC_3(t)}{dt} = k_3C_2(t) - k_4C_3(t). \qquad \text{Eq. 5}$$

Some kinetic parameters were defined as follows:

$$k_2 = \frac{K_1}{f_1V_2}, \qquad \text{Eq. 6}$$

$$k_3 = k_{on}\,B_{max}\,f_2, \qquad \text{Eq. 7}$$

$$k_4 = k_{off}. \qquad \text{Eq. 8}$$

The binding potential as described by Mintun et al. (*27*) can be defined as:

$$\text{binding potential} = \frac{B_{max}}{K_D} = \frac{1}{f_1}\frac{K_1}{k_2}\frac{k_3}{k_4}. \qquad \text{Eq. 9}$$

The two-compartment model (Fig. 1) consists of the plasma compartment (C_a) and the tissue compartment (free, nonspecifically bound and specifically bound, C_T), where rapid specific binding in comparison to the ligand transport was also assumed. The ligand concentration in the tissue compartment is given by

$$\frac{dC_T(t)}{dt} = K_1C_a(t) - k_2C_T(t). \qquad \text{Eq. 10}$$

The equilibrium distribution volume of the tissue compartment is:

$$\text{distribution volume} = \frac{1}{f_1}\frac{K_1}{k_2}, \qquad \text{Eq. 11}$$

which is progressively affected by the specific binding.

Estimation of Parameters. Four fitting configurations were used: three-compartment four-parameter fitting (3C4P); three-compartment three-parameter fitting with a fixed K_1/k_2 ratio (3C3P); three-compartment two-parameter fitting with a fixed K_1/k_2 ratio and fixed k_4 value (3C2P) and two-compartment two-parameter fitting (2C2P). The fixation of K_1/k_2 means that the free and nonspecific distribution volume (V_2) is assumed to be constant among the regions. The fixed value of the K_1/k_2 ratio was determined to be 3.00 through the study as the average of the values with 3C4P fitting in 14 of 30 cortical regions in which the ratio was reasonably small. The fixation of k_4 corresponds to assumption of a constant dissociation rate among the regions. The fixed value of k_4 was determined to be 0.026 as the average of the values in all 30 cortical regions with 3C3P fitting.

Estimation of the rate constants was performed on a personal computer by a nonlinear least-square curve-fitting procedure using a simplex algorithm (*29*). A uniform set of initial values of parameters was used in each configuration for all regions in all subjects. Input functions were derived from the lipophilic activities in the arterial plasma using numerical interpolation. The vascular activity in the ROI was neglected because it was estimated to be less than 1% in cortical regions (by an observed brain-to-blood ratio of 5.0 and an assumed CBV of 0.05 ml/g) even at 2 min after injection. The goodness of fit was evaluated by Akaike's information criteria (*30*).

Simulation Studies. Simulation studies were performed to assess the validity of two-parameter configurations. A set of six brain time-activity curves were mathematically generated using individual input functions (n = 6) and a certain parameter set (K_1 – k_4) with the 3C4P model. Multiple sets of time-activity curve(s) were generated by changing one of K_1 (with fixed K_1/k_2), $1/k_2$, k_3 and $1/k_4$ from 25% to 175% of the corresponding baseline value. The baseline values were the averages for 30 cortical regions (K_1 = 0.26, k_2 = 0.087, k_3 = 0.23 and k_4 = 0.026). Then K_1 and binding potential were estimated from the simulated time-activity curve(s) and individual input functions with 3C2P or 2C2P and compared with the original values. The effect of noise in the time-activity curve(s) was not evaluated on the simulations.

Table Look-up Procedure. Parameter estimation was also carried out by a table look-up procedure with the 3C2P configuration. This procedure required two look-up tables (Fig. 2) with which K_1 and k_3 were uniquely determined from the tissue activity in the early scan (B_E), and the late-to-early activity ratio (B_L/B_E).

The look-up tables were generated as follows: The tissue activities within the "early" and "late" SPECT scan, B_E and B_L are given by:

$$B_E = \int_{T_{E2}}^{T_{E1}} \int_0^t C_a(s)f(t-s)\,ds\,dt, \qquad \text{Eq. 12}$$

$$B_L = \int_{T_{L2}}^{T_{L1}} \int_0^t C_a(s)f(t-s)\,ds\,dt, \qquad \text{Eq. 13}$$

respectively, where T_{E1} and T_{E2} are the start- and end-time of the early scan, T_{L1} and T_{L2} those of the late scan and f(t) the transfer function given by Equations 4 and 5,

$$f(t) = \frac{K_1}{x_2 - x_1}\{(k_3 + k_4 - x_1)e^{-x_1t} + (x_2 - k_3 - k_4)e^{-x_2t}\},$$

where

$$x_{1,2} = \frac{(k_2 + k_3 + k_4) \pm \sqrt{(k_2 + k_3 + k_4)^2 - 4k_2k_4}}{2}.$$

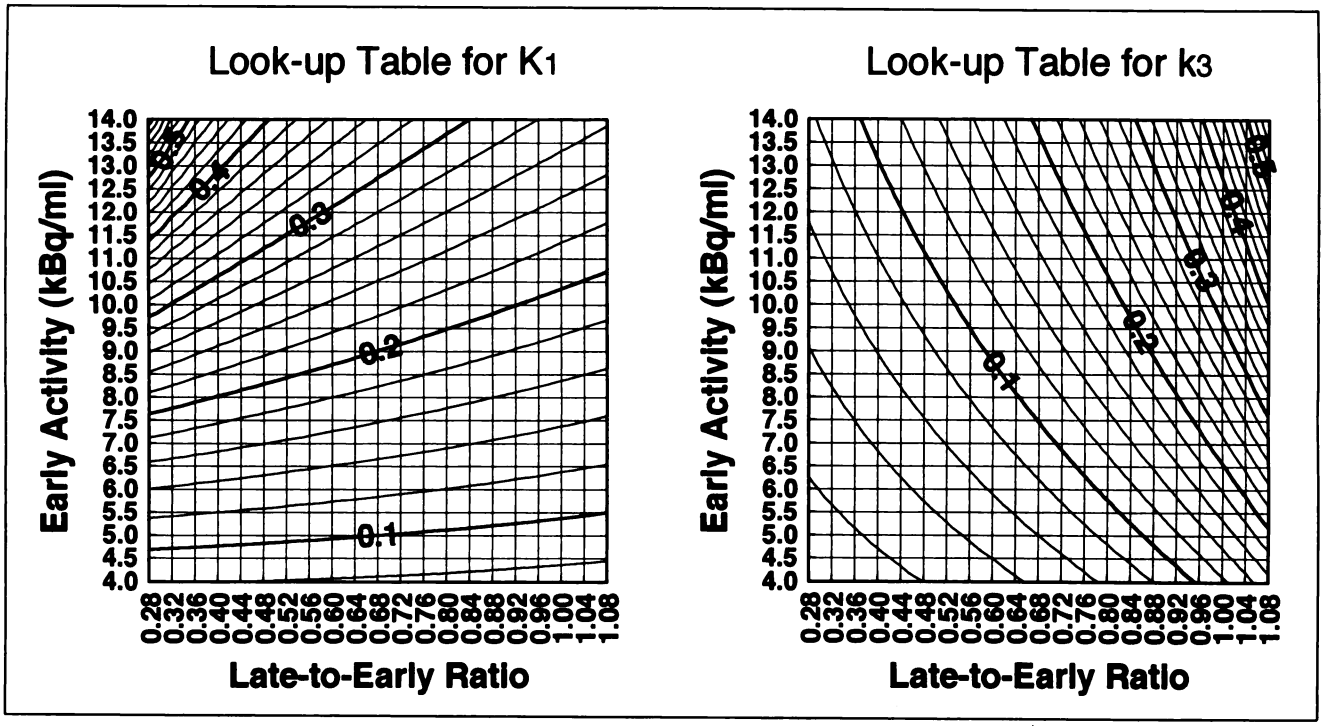

FIGURE 2. Graphical presentation of look-up tables. SPECT scan times were 12 (early scan) and 112 min after injection (late scan).

The computation of the tables consisted of the following steps:

Step 1: Possible sets of brain tissue activities within the early and late scan were calculated with an individual arterial input function and sets of K_1 and k_3 (from 0.02 to 1.00 at 0.02 intervals for both). This step gave two tables with which B_E and B_L/B_E were determined from K_1 and k_3.

Step 2: K_1 was determined by any sets of k_3 and B_E using the former table and numerical interpolation, and then B_L/B_E by the K_1 determined and k_3. This allowed the constitution of two new tables: one table gave K_1 and the other gave B_L/B_E, from k_3 and B_E.

Step 3: The objective tables were generated by the manner similar to Step 2; that is, B_E was determined by sets of K_1 and k_3, then B_L/B_E was determined.

The above procedures were carried out only once per subject. Two 16-min SPECT data images were used to determine K_1 and the binding potential. The midtime of the SPECT scan was assumed to be 12, 16 and 20 min for the early scan and 112 min for the late scan.

Parametric Images. Parametric images of K_1 and binding potential were generated by the pixel-by-pixel table look-up procedure with 3C2P on a workstation. Two 16-min SPECT images at 12 and 112 min (mid-scan time) after injection were used for calculation. K_1 and binding potential given by ROI on the parametric images were compared with those by TAC in the same ROI and 3C3P curve fitting to assess the validity of the images.

RESULTS

In general, 3C4P and 3C3P gave visually identical curve-fits in all regions. The 3C2P also gave similar curves in the cortical regions, but somewhat different curves in the regions with low receptor density, such as the pons; 2C2P gave curves different from the three-compartment configurations and they showed poorer fit with the raw data, especially in the region containing fewer receptors.

Table 2 compiles the kinetic parameter estimates with all configurations. K_1 and binding potential were well identified. The order of regional binding potential values was consistent with the known regional benzodiazepine receptor density in the human brain measured in in vitro (*31*) and by PET (*32,33*); similar K_1 values were observed in the cortical regions, thalamus, striatum and cerebellum.

3C4P identified K_1 and binding potential with coefficients of variation (CV) ranging from 13% to 21% and 7% to 25%, respectively, while large CVs and remarkable differences among the cerebral cortical regions were observed in the parameter estimates of k_2 and k_3. Moreover, a strong positive correlation ($r = 0.866$, $n = 30$, $p < 0.0001$) was observed between k_2 and k_3 in the cerebral cortical regions.

3C3P gave estimates for K_1 and binding potential which were similar to those with 3C4P. The AICs did not increase, suggesting preservation of goodness of fit. The CVs in K_1 and binding potential were not very different from those with 3C4P while those in k_3 were markedly reduced to 11%–38% from 29%–100% with 3C4P. No correlation between k_2 and k_3 in the cerebral cortical regions was observed ($r = 0.233$, $n = 30$, $p = 0.215$). Both 3C2P and 2C2P provided good estimates of the receptor density; the correlation coefficients of binding potential by 3C2P and distribution volume by 2C2P with binding potential by 3C3P were $r = 0.990$ and $r = 0.993$, respectively ($n = 60$). Since distribution volume is the sum of the nonspecific and specific distribution volumes, it is always larger than the

TABLE 2
Iodine-123-Iomazenil Kinetic Parameters for 3C4P, 3C3P, 3C2P and 2C2P Configurations

	Region									
	Frontal 1	Frontal 2	Occipital	Temporal	Parietal	Thalamus	Striatum	Cerebellum	WMV	Pons
3C4P										
K1	0.242	0.260	0.254	0.253	0.242	0.243	0.270	0.250	0.150	0.219
	(17%)*	(13%)	(13%)	(13%)	(13%)	(21%)	(12%)	(13%)	(15%)	(13%)
k2	0.048	0.082	0.047	0.057	0.071	0.063	0.085	0.053	0.061	0.120
	(61%)	(34%)	(40%)	(48%)	(30%)	(55%)	(43%)	(39%)	(50%)	(62%)
k3	0.125	0.217	0.151	0.173	0.216	0.131	0.168	0.130	0.095	0.074
	(68%)	(29%)	(60%)	(50%)	(30%)	(84%)	(58%)	(54%)	(100%)	(78%)
k4	0.026	0.026	0.026	0.030	0.028	0.035	0.038	0.031	0.019	0.019
	(23%)	(17%)	(26%)	(25%)	(14%)	(74%)	(17%)	(15%)	(33%)	(30%)
BP	94	114	120	111	109	55	54	78	43	28
	(11%)	(7%)	(14%)	(12%)	(7%)	(23%)	(6%)	(13%)	(25%)	(8%)
%NSB	23	11	18	17	12	27	22	22	22	25
	(55%)	(35%)	(50%)	(46%)	(35%)	(45%)	(44%)	(27%)	(33%)	(35%)
AIC	55.1	55.4	61.3	55.7	53.6	75.7	71.2	57.3	64.5	75.1
	(9%)	(14%)	(14%)	(11%)	(10%)	(6%)	(4%)	(7%)	(10%)	(9%)
3C3P										
K1	0.260	0.264	0.274	0.268	0.249	0.253	0.277	0.267	0.152	0.192
	(16%)	(12%)	(15%)	(15%)	(15%)	(24%)	(17%)	(18%)	(21%)	(15%)
k3	0.225	0.229	0.258	0.262	0.235	0.194	0.189	0.214	0.058	0.036
	(19%)	(13%)	(15%)	(22%)	(12%)	(30%)	(16%)	(11%)	(23%)	(38%)
k4	0.027	0.025	0.025	0.028	0.026	0.046	0.042	0.032	0.017	0.016
	(15%)	(14%)	(16%)	(22%)	(14%)	(46%)	(23%)	(20%)	(21%)	(40%)
BP	105	116	129	119	112	56	57	85	45	28
	(7%)	(8%)	(12%)	(9%)	(7%)	(15%)	(13%)	(19%)	(30%)	(12%)
%NSB	11	10	9	10	10	19	18	13	23	31
	(6%)	(7%)	(10%)	(8%)	(6%)	(13%)	(10%)	(15%)	(25%)	(9%)
AIC	55.7	53.8	62.3	56.8	52.3	75.4	70.3	58.1	60.3	75.7
	(7%)	(15%)	(10%)	(10%)	(10%)	(6%)	(5%)	(8%)	(11%)	(8%)
3C2P										
K1	0.261	0.261	0.272	0.270	0.249	0.270	0.300	0.275	0.146	0.186
	(16%)	(11%)	(14%)	(15%)	(15%)	(20%)	(16%)	(17%)	(20%)	(17%)
k3	0.220	0.238	0.266	0.247	0.233	0.126	0.130	0.183	0.077	0.045
	(8%)	(7%)	(12%)	(9%)	(6%)	(12%)	(11%)	(16%)	(26%)	(22%)
BP	106	114	128	119	112	60	63	88	37	22
	(8%)	(7%)	(12%)	(9%)	(6%)	(12%)	(11%)	(16%)	(26%)	(22%)
%NSB	11	10	9	10	10	17	17	13	26	37
	(7%)	(7%)	(11%)	(8%)	(6%)	(10%)	(9%)	(13%)	(21%)	(14%)
AIC	54.7	52.7	60.9	55.9	51.5	74.8	72.1	57.4	61.7	75.5
	(6%)	(16%)	(10%)	(11%)	(10%)	(7%)	(5%)	(4%)	(9%)	(8%)
2C2P										
K1	0.204	0.208	0.217	0.213	0.199	0.197	0.215	0.209	0.118	0.143
	(13%)	(9%)	(13%)	(13%)	(12%)	(16%)	(12%)	(14%)	(18%)	(13%)
k2	0.008	0.007	0.007	0.007	0.007	0.013	0.014	0.010	0.011	0.020
	(10%)	(3%)	(10%)	(8%)	(9%)	(11%)	(12%)	(10%)	(15%)	(5%)
DV	110	118	133	124	116	65	66	92	44	30
	(7%)	(9%)	(12%)	(8%)	(6%)	(11%)	(10%)	(16%)	(20%)	(13%)
AIC	68.2	69.4	69.4	67.8	64.9	79.1	76.8	70.3	73.3	85.4
	(7%)	(7%)	(8%)	(9%)	(11%)	(7%)	(6%)	(7%)	(7%)	(8%)

*Numbers in parentheses are coefficients of variance.

WMV = white matter/ventricle; BP = binding potential; %NSB = percent of nonspecific binding; AIC = Akaike's information criteria; DV = distribution volume. Units = ml/min/ml for K1; 1/min for k2, k3 and k4; and ml/ml for BP and DV.

Values are the mean and coefficient of variance (cv = sd/mean) for parameter estimates.

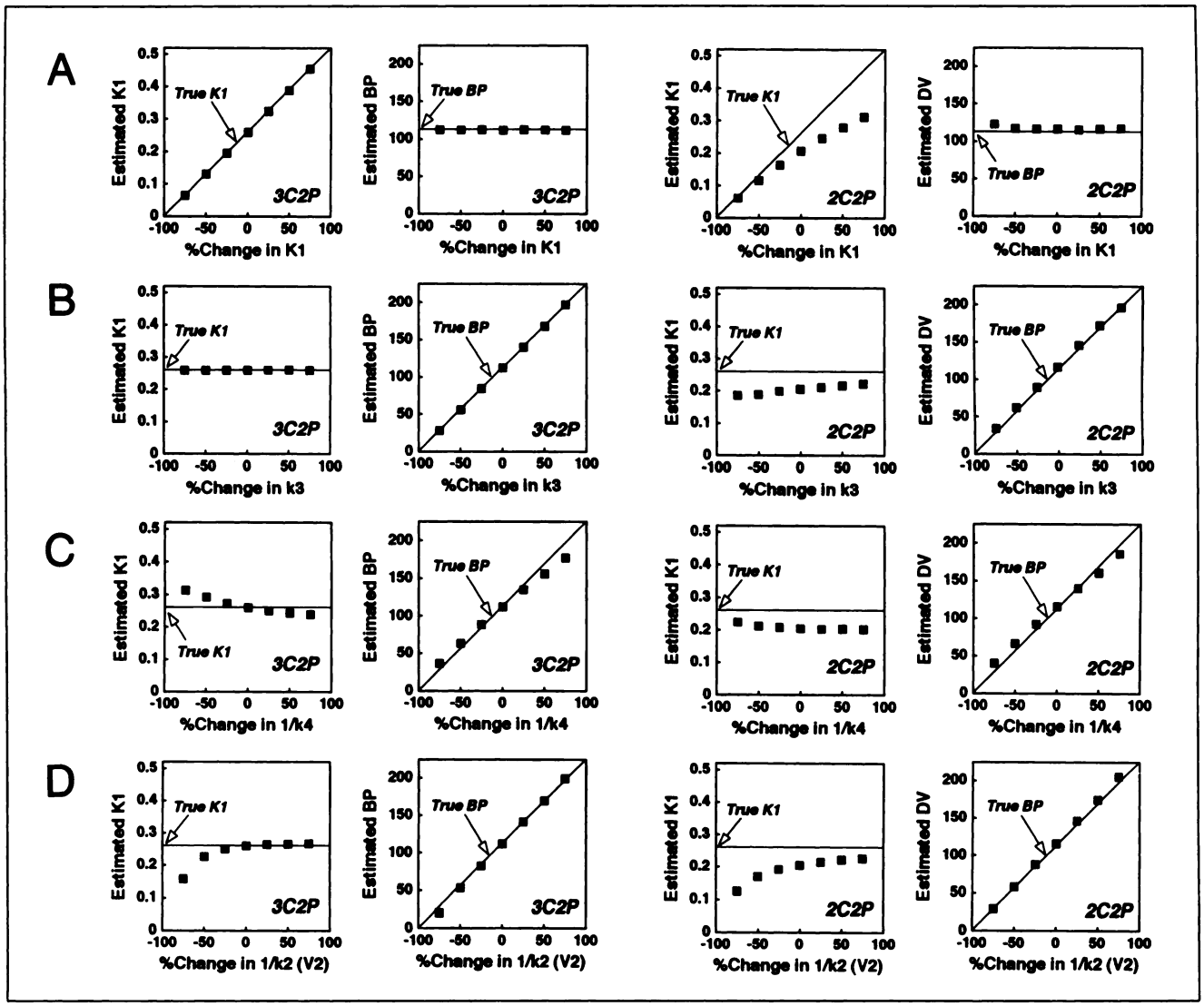

FIGURE 3. Relation between the estimated and true parameters are shown for K_1 and binding potential with 3C2P and for K_1 and distribution volume with 2C2P, from left to right. Although each study included six simulations, the standard deviations were always nearly zero, and only the mean values were plotted. (a) Effect of change in K_1 with fixed K_1/k_2 (3.00), which corresponds to the change in the blood flow. 3C2P provided correct estimates, while 2C2P gave smaller K_1 as true K_1 increased. (b) Effect of change in k_3 which corresponds to the change in receptor density. 3C2P provided correct estimates, while 2C2P gave slightly smaller K_1 as k_3 reduced. (c) Effect of change in $1/k_4$ which corresponds to change in the inverse of the dissociation rate (predominantly the affinity). The results by 3C2P were significantly affected, and smaller/larger K_1 and larger/smaller binding potential were given as $1/k_4$ increased/decreased. While 2C2P showed the same trends, the error in K_1 was less. (d) Effect of change in $1/k_2$ corresponding to the change in nonspecific distribution volume (V_2). Both 3C2P and 2C2P gave remarkably smaller K_1 and almost correct binding potential as $1/k_2$ decreased, while they gave quite stable results when $1/k_2$ increased.

binding potential. 3C2P also provided good estimates of K_1 ($r = 0.982$, $n = 60$), whereas 2C2P consistently gave lower values for K_1 ($r = 0.977$, $n = 60$, but 28% lower than K_1 by 3C3P). AICs did not increase with 3C2P, whereas they were obviously increased with 2C2P.

Figure 3 shows the results of the simulation studies, which delineate the differences between 2C2P and 3C2P in detail. 3C2P provided perfect estimations for K_1 and binding potential against the changes in K_1 and k_3, where the assumptions of the configuration were met. On the other hand, 2C2P gave good distribution volume but markedly lower K_1 estimates with the true K_1 becoming higher (high flow). In addition, estimates of K_1 by 2C2P were affected by the change in k_3. K_1 estimates by 3C2P were markedly affected by the change in $1/k_4$, where assumptions of the configuration were not met, while binding potential was rather stable. K_1 and distribution volume by 2C2P fitting were relatively stable against the change in $1/k_4$. Both configurations showed similar responses to the change in $1/k_2$ (proportional to V_2, the nonspecific binding), i.e., K_1 was markedly underestimated at <50% of the V_2 values, while binding potential was correctly estimated.

The estimates of K_1 and binding potential given by the data at two points (12 and 112 min postinjection) and the

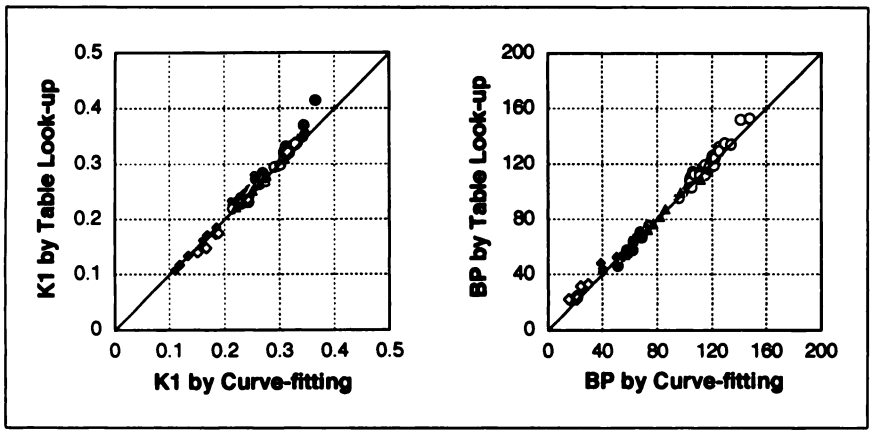

FIGURE 4. Correlation between parameter estimates by the table look-up and curve-fitting procedure with the 3C2P configuration. Two datasets for each region at 12 and 112 min after ligand injection were used in the table look-up procedure. The data acquisition time was assumed to be 16 min for the early and late scans. Open circles = cerebral cortex; closed circles = thalamus and striatum; closed triangles = cerebellum; open diamonds = pons; closed diamonds = white matter/ventricle.

table look-up procedure with the 3C2P configuration correlated well with those from the whole 27 SPECT data and curve fitting, as demonstrated in Figure 4. The delay in the early scan time (16 and 20 min) also provided quite similar binding potential estimates in all regions, as well as similar K_1 in the cortical regions and cerebellum. Higher and lower K_1 were given in the deep gray matter and pons/WMV, respectively, with less than 5% error. Parametric images generated by the table look-up procedure (Fig. 5) also provided good estimates of K_1 and binding potential (Fig. 6).

DISCUSSION

Alterations of benzodiazepine receptors have been reported in such pathological states as epilepsy (*34–36*), Alzheimer's disease (*37,38*), Huntington's disease (*39–41*), schizophrenia (*42–44*) and ischemia (*45*). Sette et al. (*46*) demonstrated preserved benzodiazepine receptor density with suppressed blood flow and oxygen consumption in the noninfarcted area in the baboon after transient ischemia using PET. Their findings suggest the potential application of measurement of the benzodiazepine receptor density as a marker of the neuronal density in various disorders.

Iodine-123-iomazenil SPECT with compartmental analysis is a potential method for measuring ligand transport (K_1) and benzodiazepine receptor density (binding potential or distribution volume) at the same time. Ligand transport is affected predominantly by the blood flow, and K_1 may be used as a marker of the cerebral blood flow (CBF) in clinical settings. Combination of K_1 and binding potential may permit assessment of the balance of the CBF and the neuronal density.

Abi-Dargham et al. (*25,26*) documented compartment analysis with [^{123}I]iomazenil and SPECT in healthy humans. Our results are quite consistent with theirs in terms of the relative distribution of parameters. The absolute values of estimated K_1 and binding potential in the present study were less than their previous report (*25*) but were compatible with their more recent one (*26*) except for the value of f_1 fraction.

Quantification of neuroreceptors by compartmental model analysis usually requires a long dynamic data acquisition time and frequent arterial sampling. Since [^{123}I]iomazenil can be used in many nuclear medicine facilities with SPECT, a simplified procedure for quantitative measurement of benzodiazepine receptors would have significant clinical value. Simplification of the SPECT acquisition may be achieved by two strategies: shortening of the scanning time and reduction of the number of scans. Unfortunately, [^{123}I]iomazenil demonstrates slower washout from the brain, and it was reported that at least 60 min of SPECT data were required to yield stable parameter estimates (*25*). We reached a similar conclusion in this study (data not shown). Therefore, we tested another strategy in which two parameters could be estimated from two SPECT data.

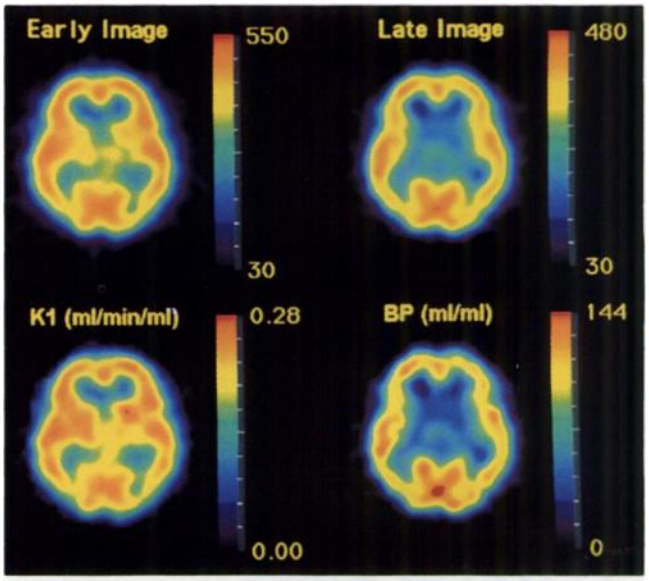

FIGURE 5. Early and late SPECT images (upper) and parametric images of K_1 and binding potential generated from the two SPECT images by the table look-up procedure and 3C2P configuration (lower) in a representative subject. The early and late SPECT images were reconstructed using 4–20 min and 104–120 min data after injection of the ligand. The K_1 image had a strong resemblance to known blood flow images, in which the deep structures such as the thalamus and striatum were more clearly seen than in the early SPECT image. The binding potential images were similar to the late images.

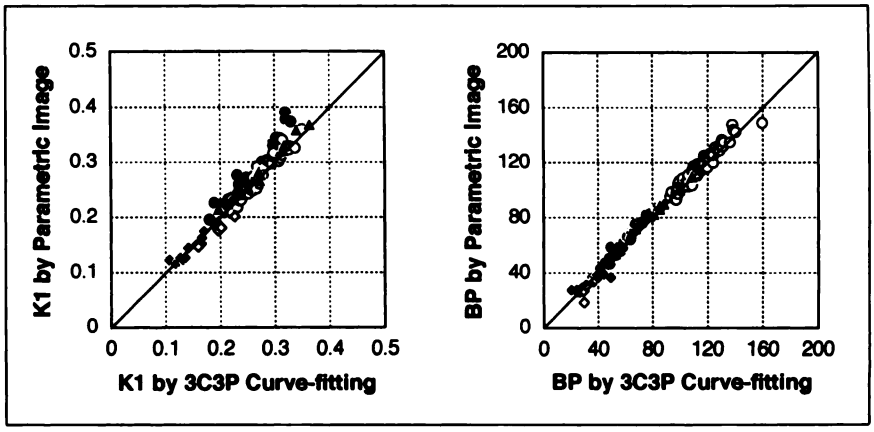

FIGURE 6. Relation between parameter estimates from the parametric images (Fig. 5) and the 3C3P curve fitting using the same ROIs. Estimates obtained by both methods showed good correlation.

To develop a simplified technique for quantification of [^{123}I]iomazenil SPECT, we first compared four configurations of the compartmental model, that is, 3C4P, 3C3P, 3C2P and 2C2P. In general, all configurations provided reasonably acceptable K_1 and binding potential (distribution volume) values: similar K_1 values were obtained in the cerebral cortex, cerebellum, thalamus and striatum, and the order of regional binding potential (or distribution volume) values was consistent with the known benzodiazepine receptor density (*31–33*). A significant amount of distribution volume measured in the regions with a lack of benzodiazepine receptors, such as the pons and white matter, was probably due to the scattered radiation and the limited spatial resolution of the SPECT images.

The most complex configuration, 3C4P, gave larger intersubjective and interregional variations in parameter estimates of k_2 and k_3, even in the cortical regions, and a strong correlation between the two parameter estimates. These results suggest that the number of parameters is too large for the statistical quality of these studies.

3C3P is derived by assuming the free and the nonspecific distribution volume to be constant among the regions. We assumed a uniform value, 3.00, for K_1/k_2 in all the subjects. This value gave a nonspecific binding fraction of about 10% in the cortical region, which is roughly comparable to the values previously reported in humans with the displacement study (*2*) and with compartment model analysis in the equilibrium state (*25*). 3C3P well identified three individual parameters, K_1, k_3, and k_4, with reasonably small CVs. K_1 and binding potential by 3C3P were close to those by 3C4P. These findings support the validity of applying a uniform K_1/k_2 value to all of the subjects, and we regarded the results from the 3C3P configuration as the reference standard in the considerations below.

Further simplification was attempted using the 3C2P and 2C2P configurations. The former model was derived by assuming a uniform dissociation rate (k_4) in all regions and subjects, while the latter model was derived by assuming the specific binding to be rapid compared with the ligand transport.

3C2P provided parameter estimates very close to those with 3C3P. Although slight under- or overestimation occurred for the deep gray matter, white matter and pons simply because the mean value of k_4 in the cortical regions was used in the other regions, the degree of error was acceptable and these results support the validity of this configuration for the normal brain.

2C2P also provided good estimation of the receptor density (distribution volume) unless the degree of the curve fitting was not as good as 3C2P. The ligand transport (K_1), however, was markedly underestimated. The reason for this underestimation is probably that the specific binding is not very rapid and thus cannot be included in a single compartment, as described by Koeppe et al. (*21*) with [^{11}C]flumazenil.

The simulation studies further characterized the differences between these two simplified configurations. Both configurations generally gave good estimates of the receptor density. When the ligand transport (K_1) and/or the receptor density (k_3) changes, and when nonspecific binding increases (k_2 decreases), 3C2P provided more correct estimates of K_1 than 2C2P. In contrast, 2C2P provided more reliable estimates than 3C2P did when k_4 (k_4 represents the dissociation rate constant (k_{off}) and is thus strongly related to ligand-receptor affinity) changed. Unchanged K_D has been reported in patients with epilepsy (*35*) and in rats under antipsychiatric treatment (*47*) and, to our knowledge, specific changes in the affinity of benzodiazepine receptors have not been reported.

The substantial limitation of 2C2P is that the degree of the underestimation of K_1 depends on the magnitude of K_1 itself. Underestimation of the blood flow and overestimation of the neuronal density (receptor density/ligand transport) may occur when using K_1 as a marker of the blood flow and distribution volume as a marker of the neuronal density. Therefore, 3C2P is recommended for diseases in which little change in the affinity is expected, such as ischemia and degenerative diseases, while 2C2P is recommended if the affinity is expected to change, for example, in patients on benzodiazepine medication.

Once the number of independent variables is reduced to two, both the ligand transport and the receptor density can be estimated using a precalculated look-up table with the 2-parameter model (*48*). In contrast to the standard curve-

fitting procedure which usually requires serial rapid SPECT data over quite a long time, one can get not only regional kinetic parameters but also parametric images using only two SPECT images. The estimates of K_1 and binding potential determined by the look-up procedure with the 3C2P configuration were identical to those by the curve-fitting method, and similar estimates were obtained even if the scan time varied, suggesting the possible application to conventional rotating SPECT devices. Moreover, parametric images for K_1 and binding potential were easily obtained, and they also provided good parameter estimates. All these findings support the validity of this methodology.

Of course, there are some practical problems to be solved before this method can be applied routinely. For example, the registration of two separate SPECT images and the need for frequent arterial blood sampling. The former problem has been extensively studied by many investigators (*49–51*). Concerning the latter, dramatic simplification would be possible if external monitoring of the blood activity is feasible, or standardized input function is successfully determined as demonstrated by Iida et al. (*48,52*) with [^{123}I]N-isopropyl-p-iodoamphetamine.

CONCLUSION

Iodine-123-iomazenil SPECT imaging with compartmental analysis was used for simultaneous determinations of ligand transport and receptor density. Simplification of the model by reducing the number of individual parameters to two allowed the quantification of benzodiazepine receptors on the basis of only two SPECT scans. Combining the 3C2P configuration and the table look-up procedure provided reasonably accurate parameter estimates and may allow the application with conventional rotating SPECT, which would be useful for quantitative assessment of benzodiazepine receptors in clinical settings.

REFERENCES

1. Holl K, Deisenhammer E, Dauth J, et al. Imaging benzodiazepine receptors in the human brain by SPECT. *Nucl Med Biol* 1989;16:759–763.
2. Beer HF, Blauenstein PA, Hasler PH, et al. In vitro and in vivo evaluation of iodine-123-Ro 16-0154: a new imaging agent for SPECT investigations of benzodiazepine receptors. *J Nucl Med* 1990;31:1007–1014.
3. Johnson EW, Woods SW, Zoghbi S, et al. Receptor binding characterization of the benzodiazepine radioligand ^{125}I-Ro16-0154: potential probe for SPECT brain imaging. *Life Sci* 1990;47:1535–1546.
4. Innis R, Zoghbi S, Johnson E, et al. SPECT imaging of the benzodiazepine receptor in non-human primate brain with [^{123}I]Ro 16-0154. *Eur J Pharmacol* 1991;193:249–252.
5. Innis RB, Al-Tikriti MS, Zoghbi SS, et al. SPECT imaging of the benzodiazepine receptor: feasibility of in vivo potency measurements from stepwise displacement curves. *J Nucl Med* 1991;32:1754–1761.
6. Woods SW, Seibyl JP, Goddard AW, et al. Dynamic SPECT imaging of the benzodiazepine receptor in healthy human subjects with [^{123}I]Ro 16-0154. *Psychiatry Res: Neuroimaging* 1992;45:67–77.
7. van Huffelen AC, van Isselt JW, van Veelen CWM, et al. Identification of the side of the epileptic focus with ^{123}I-iomazenil SPECT. A comparison with ^{18}FDG-PET and ictal EEG findings in patients with medically intractable complex partial seizures. *Acta Neurochir* 1990;50:(suppl)95–99.
8. Ferstl FJ, Cordes M, Cordes I, et al. Iodine-123-iomazenil SPECT in patients with focal epilepsies–a comparative study with ^{99m}Tc-HMPAO-SPECT, CT and MR. *Adv Exp Med Biol* 1991;287:405–412.
9. Schubiger PA, Hasler PH, Beer-Wohlfahrt H, et al. Evaluation of a multicentre study with iomazenil—a benzodiazepine receptor ligand. *Nucl Med Commun* 1991;12:569–582.
10. Cordes M, Henkes H, Ferstl F, et al. Evaluation of focal epilepsy: a SPECT scanning of 123-I-iomazenil versus HMPAO. *Am J Neuroradiol* 1992;13: 249–253.
11. Haldemann RC, Bicik I, Pfeiffer A, et al. Iodine-123-iomazenil: a quantitative study of the central benzodiazepine receptor distribution. *Nucl Med* 1992;31:91–97.
12. Bartenstein P, Ludolph A, Schober O, et al. Benzodiazepine receptors and cerebral blood flow in partial epilepsy. *Eur J Nucl Med* 1991;18:111–118.
13. Pappata S, Samson Y, Chavoix C, et al. Regional specific binding of [^{11}C]RO 15 1788 to central type benzodiazepine receptors in human brain: quantitative evaluation by PET. *J Cereb Blood Flow Metab* 1988;8:304–313.
14. Persson A, Ehrin E, Eriksson L, et al. Imaging of [^{11}C]-labeled RO 15-1788 binding to benzodiazepine receptors in the human brain by positron emission tomography. *J Psychiatr Res* 1985;19:609–622.
15. Iyo M, Itoh T, Yamasaki T, et al. Quantitative in vivo analysis of benzodiazepine binding sites in the human brain using PET. *Neuropharmacology* 1991;30:207–215.
16. Brouillet E, Chavoix C, Khalili-Varasteh M, et al. Quantitative evaluation of benzodiazepine receptors in live papio papio baboons using PET. *Mol Pharmacol* 1990;38:445–450.
17. Abadie P, Baron JC, Bisserbe JC, et al. Central benzodiazepine receptors in human brain: estimation of regional Bmax and K_D values with PET. *Eur J Pharmacol* 1992;213:107–115.
18. Blomqvist G, Pauli S, Farde L, et al. Maps of receptor binding parameters in the human brain—a kinetic analysis of PET measurements. *Eur J Nucl Med* 1990;16:257–265.
19. Laruelle M, Abi-Dargham A, Rattner Z, et al. SPECT measurement of benzodiazepine receptor number and affinity in primate brain: a constant infusion paradigm with [^{123}I]iomazenil. *Eur J Phamacol* 1993;230:119–123.
20. Laruelle M, Abi-Dargham A, Al-Tikriti MS, et al. SPECT quantification of [^{123}I]iomazenil binding to benzodiazepine receptors in nonhuman primates. II. Equilibrium analysis of constant infusion experiments and correlation with in vitro parameters. *J Cereb Blood Flow Metab* 1994;14:453–465.
21. Koeppe RA, Holthoff VA, Frey KA, et al. Compartmental analysis of [^{11}C]Flumazenil kinetics for the estimation of ligand transport rate and receptor distribution using PET. *J Cereb Blood Flow Metab* 1991;11:735–744.
22. Holthoff VA, Koeppe RA, Frey KA, et al. Differentiation of radioligand delivery and binding in the brain: validation of a two-compartment model for [^{11}C]flumazenil. *J Cereb Blood Flow Metab* 1991;11:745–752.
23. Frey KA, Holthoff VA, Koeppe RA, et al. Parametric in vivo imaging of benzodiazepine receptor distribution in human brain. *Ann Neurol* 1991;30: 663–672.
24. Laruelle M, Baldwin RM, Rattner Z, et al. SPECT quantification of [^{123}I] iomazenil binding to benzodiazepine receptors in nonhuman primates. I. Kinetic modeling of single bolus experiments. *J Cereb Blood Flow Metab* 1994;14:439–452.
25. Abi-Dargham A, Laruelle M, Seibyl J, et al. SPECT measurement of benzodiazepine receptors in human brain with [^{123}I]iomazenil: kinetic and equilibrium paradigms. *J Nucl Med* 1994;35:228–238.
26. Abi-Dargham A, Gandelman M, Zoghbi SS, et al. Reproducibility of SPECT measurement of benzodiazepine receptors in human brain with [^{123}I]iomazenil. *J Nucl Med* 1995;36:167–175.
27. Mintun MA, Raichle ME, Kilbourn MR, et al. A quantitative model for the in vivo assessment of drug binding sites with positron emission tomography. *Ann Neurol* 1984;15:217–227.
28. Zoghbi SS, Baldwin RM, Seibyl JP, et al. Pharmacokinetics of the SPECT benzodiazepine receptor radioligand [^{123}I]iomazenil in human and nonhuman primates. *Nucl Med Biol* 1992;19:881–888.
29. Nelder JA, Mead R. A simplex method for function minimization. *Computer J* 1965;7:308–312.
30. Akaike H. A new look at the statistical model identification. *IEEE Trans Automat Contr* 1974;AC19:716–723.
31. Richards JG, Mohler H. Benzodiazepine receptors. *Neuropharmacology* 1984;23:233–242.
32. Samson Y, Hanatraye P, Baron JC, et al. Kinetics and displacement of [^{11}C]Ro 15-1788, a benzodiazepine antagonist, studied in human brain in vivo by PET. *Eur J Pharmacol* 1985;110:247–251.
33. Shinoto H, Yamasaki T, Inoue O, et al. Visualization of specific binding sites of benzodiazepine in human brain. *J Nucl Med* 1986;27:1593–1599.
34. Roy A, Bakay E, Harris A. Neurotransmitter, receptor and biochemical changes in monkey cortical epileptic foci. *Brain Res* 1980;206:387–404.

35. Savic I, Persson A, Roland P, et al. In vivo demonstration of reduced benzodiazepine receptor binding in human epileptic foci. *Lancet* 1988;30: 863–866.
36. Johnson EW, de Lanerolle NC, Kim JH, et al. Central and peripheral benzodiazepine receptors: opposite changes in human epileptogenic tissue. *Neurology* 1992;42:811–815.
37. Owen F, Poulter M, Waddinton JL, Mashal RD, Crow TJ. [^{3}H]-Ro 05-4864 and [^{3}H]flunitrazepam binding in kainate-lesioned rat striatum and temporal cortex of brains from patients with senile dementia of the Alzheimer type. *Brain Res* 1983;278:373–375.
38. Shimoshima S, Taniguti T, Fujiwara M, Kameyama M. Change in benzodiazepine receptors in Alzheimer type dementia. *Ann Neurol* 1988;23:404–406.
39. Penney JB, Young AB. Quantitative autoradiography of neurotransmitter receptors in Huntington disease. *Neurology* 1982;32:1391–1395.
40. Walker FO, Young AB, Penney JB, Dovorini-Zis K, Shoulson I. Benzodiazepine and GABA receptors in early Huntington's disease. *Neurology* 1984;34:1237–1240.
41. Whitehouse PJ, Trifiletti RR, Jones BE, et al. Neurotransmitter receptor alterations in Huntington's disease: autoradiographic and homogenate studies with special reference to benzodiazepine receptor complex. *Ann Neurol* 1985;18:202–210.
42. Kiuchi Y, Kobayashi T, Takeuchi J, et al. Benzodiazepine receptors increase in postmortem brain of chronic schizophrenics. *Eur Arch Psychiatr Neurol* 1989;239:71–78.
43. Benes FM, Vincent SL, Alsterberg G, Bird ED, SanGiovanni JP. Increased GABAa receptor binding in superficial layers of cingulate cortex in schizophrenics. *J Neurosci* 1992;12:924–929.
44. Squires RF, Lajtha A, Seaderup E, Palkovits M. Reduced [3H]flunitrazepam binding in cingulate cortex and hippocampus of postmortem schizophrenic brains: is selective loss of glutamatergic neurons associated with major psychoses? *Neurochem Res* 1993;18:219–223.
45. Onodera H, Sato G, Kogure K. GABA and benzodiazepine receptors in the gerbil brain after transient ischemia: demonstration by quantitative receptor autoradiography. *J Cereb Blood Flow Metab* 1987;7:82–88.
46. Sette G, Baron JC, Young AR, et al. In vivo mapping of brain benzodiazepine receptor changes by PET after focal ischemia in the anesthetized baboon. *Stroke* 1993;24:2046–2058.
47. Rupniak NMJ, Prestwich SA, Horton RW, Jenner P, Marsden CD. Alterations in cerebral glutamic acid decarboxylase and 3H-flunitrazepam binding during continuous treatment of rats up to 1 yr with haloperidol, sulpiride or clozapine. *J Neural Transm* 1978;68:113–125.
48. Iida H, Itoh H, Bloomfield P, et al. A method to quantitate CBF using a rotating gamma camera and I-123-amphetamine (IMP) with one blood sampling. *Eur J Nucl Med* 1994;21:1072–1084.
49. Minoshima S, Berger KL, Lee KS, Mintun MA. An automated method for rotational correction and centering of three-dimensional functional brain images. *J Nucl Med* 1992;33:1579–1585.
50. Hoh CK, Dahlbom M, Harris G, et al. Automated iterative three-dimensional registration of positron emission tomography images. *J Nucl Med* 1993;34:2009–2018.
51. Rusinek H, Tsui WH, Levy AV, Noz ME, de Leon MJ. Principal axes and surface fitting methods for three-dimensional image registration. *J Nucl Med* 1993;33:2019–2024.
52. Iida H, Itoh H, Nakazawa M, Nishimura H, Onishi Y, Uemura K. Quantitative mapping of regional cerebral blood flow using iodine-123-IMP and SPECT. *J Nucl Med* 1994;35:2019–2030.